Control of copper nanoparticle metallization on electrospun fibers via Pd and Ag seed-assisted templating

Temitope Q. Aminu (taminu@purdue.edu), David F. Bahr (dfbahr@purdue.edu)

School of Materials Engineering, Purdue University, West Lafayette, IN 47907, U.S.A.

Author accepted version, Journal of Materials Science, vol. 56, pp 16307-16323(2021)
DOI: 10.1007/s10853-021-06326-x

ABSTRACT

We investigated the effects of palladium and silver seed chemistries on the electroless deposition of copper nanoparticles on electrospun polyacrylonitrile (PAN) fibers to identify conditions that enable formation of either conformal coatings or isolated metallic nanoparticles. The kinetics of Cu deposition was enhanced on Pd seeded fibers over Ag seeding, and continuous growth of copper nanoparticles conformal to the PAN fibers was achieved in instances with high seed density for both seed chemistries. A discrete distribution of copper nanoparticles was observed for low density silver seeding. Furthermore, the high density Ag seeds promoted dense and compact copper nanoparticle films, while the films on the Pd seeded fibers were rough with inclusions of microporosity. Raman spectroscopy revealed that a higher ratio of the D to G bands formed during processing, indicative of more cyclization of nitrile groups in surface PAN molecules during the seeding and deposition processes, corresponds to a higher seeding density. Thermal stability of PAN is enhanced with isolated Pd seeds present where the seed size is lower than the mean free path for electron conduction, but degrades as larger seeds or more dense and compact metallic shells are formed on the fibers.

Keywords: Electrospinning; Polymer fibers; Electroless deposition; Copper nanoparticles Silver mirror reaction; Two – step activation

INTRODUCTION

The directed assembly of metallic nanostructures on micron and submicron-sized features serves two primary purposes: first, to mitigate structural coalescence between individual nanoparticles, an inevitable consequence of the spontaneous driving force to reduce the high surface free energies intrinsic to nanomaterials; and secondly, to confine the growth of these metallic species on appropriate substrates so as to exploit distinctive properties, such as electron transport, optical, magnetic and catalytic properties that these nanomaterials possess for various functional applications. Polymeric materials, due to their molecular configuration, relative ease of structural modification, and overall chemical stability play a pivotal role in the synthesis and stabilization of metallic nanoparticles(NPs) [1]. The polymer matrix often either serves as a medium for dispersion of pre-formed metallic nanoparticles [2], or utilized as a micro-reactor for in-situ synthesis [1, 3]. In both cases, nanoparticle stability is achieved through steric hindrance from the polymer chains. However, a corollary of these processes is that a substantial number of the nanoparticles are permanently embedded in the polymer, and occluded from the functional environment. This renders the material design less efficient for applications in which the nanoparticle must make contact with fluids or gases, and may lead to either additional costs or an unexpected change in the properties of the fibers with embedded particles (such as an increase in stiffness). Hence, methods for creating surface-confined nanoparticle synthesis are of practical importance.

Electrospinning has become a widely used technique for the generation of polymer fibers with diameters ranging from a few nanometers to several microns [4]. Electrospun fibers possess high-aspect ratios and high surface area – to – volume ratios, and coupled with the amenable chemistry of the underlying polymer, represent model materials for substrate-confined templating of metallic nanostructures. In addition to stabilization, surface confinement ensures that these nanoparticles are continuously exposed to their intended functional environments. Metallic nanoparticles supported on electrospun fibers have been utilized in a broad range applications including water filtration membranes, biosensor design [5], superhydrophobic separation membranes [6], Surface-enhanced Raman spectroscopy substrates [7], and antibacterial fibers [8, 9].

The fabrication and adoption of nanocomposites based on incorporation of cuprous species has been fostered by a myriad facile copper nanoparticle synthesis methodologies, making them versatile functional materials for use in diverse fields [10]. Numerous procedures have been

developed for fabrication methods that exclusively immobilize metallic NPs on electrospun fibers. For instance, gold and silver NPs were grafted to polyvinyl alcohol (PVA) fibers utilizing bio-inspired catechol moieties [11]. In the same vein, platinum and silver NPs were assembled on Nylon 6 nanofibers by interfacial hydrogen reactions between citrate stabilizers and the amide functional groups on the polymer chain [12]. Silver NPs were deposited on polyacrylonitrile (PAN) fibers through coaxial electrospinning and subsequent exposure to ultraviolet irradiation [9]. For copper NPs deposition, however, the electroless protocol has been broadly adopted [13, 14]. Electroless deposition encompasses all "wet-chemistry" deposition techniques whose working principles are founded on spontaneous electrochemical redox reactions. Traditional formulations consist of a metal salt, a complexing agent, a reducing agent and suitable additives for process control. In general, this technique affords excellent throwing power, flexible control over deposit properties and morphology, and a relatively simple mode of operation [15]. In most practical cases, the fibers are pretreated with seed crystals of select transition and noble metals to facilitate subsequent nucleation and growth of copper NPs. Catalytic nuclei of palladium and silver are often utilized, deployed via various seeding strategies [16-19]. In combination with their cost-effectiveness, the underlying electrochemistry of the deposition process justifies the utility of these two species: traditionally, the anodic or oxidative reaction in electroless deposition proceeds, firstly, through activation of the reducing agent by dehydrogenation, creating electroactive species that effect metal reduction with a concomitant evolution of hydrogen gas [20]; and advantageously, silver and palladium possess affinity for hydrogen, and offer practical exchange current densities for hydrogen gas evolution, promoting rapid anodic reaction kinetics [21].

A classic method for palladium seeding is the two-step sensitization-activation process for plating non-conductive substrates based on the electrochemistry of mixtures of tin and palladium salts [20]. There is a litany of working formulations documented in patents and literature that contain essentially variable proportions of tin(II) chloride ($SnCl_2$) and palladium chloride ($PdCl_2$) as the active ingredients [22]. In a copper NP metallization procedure, the fibers are first sensitized in the tin(II) chloride bath, and subsequently activated in a palladium chloride bath, inducing the precipitation of palladium seeds on the fiber surface that catalyze copper deposition [23]. On the other hand, for silver seeding, the well-known silver mirror reaction based on the redox processes between silver salt and an aldehyde e.g. glucose, offers a simple and straightforward, but surprisingly underutilized, method for the Ag-facilitated deposition of copper NPs on electrospun fibers.

In this study, we have conducted a systematic study on the seeding chemistry, size and density on the electroless deposition of copper on electrospun PAN fibers to determine processing conditions which allow the creation of either continuous conformal coatings or isolated metallic nanoparticles. While we recognize that embedding particles within fibers may reduce processing steps during metallization [24], the additional complexity of forming particles during the spinning process adds process costs that we believe are roughly equivalent to seeding processes in electroless deposition. Polyacrylonitrile is a hydrophilic polymer that possesses good thermal and chemical stability, and it's derived fibers are used in medical and industrial applications [25]. In addition, the active polar nitrile groups in the PAN molecule aid the introduction of additional functional groups [26] that support metal (seed) adsorption during electroless deposition. We have demonstrated control over Ag seeding density and particle size with the silver mirror reaction, and how copper NP continuity and conformity with the underlying PAN fiber are guided by the seeding density. We evaluate differences in the copper NP film morphology and conformity derived from the silver and palladium seeded fibers. Scanning electron microscopy and X-ray diffraction results show differences in resultant microstructures and deposition kinetics of copper NP. Raman spectroscopy shows clear modification in the fiber surface chemistry with immersion in the metallization baths. Thermogravimetric analysis shows an overall degradation in the thermal stability of PAN fibers as a resulting from metallic nanoparticle immobilization. In addition, a more efficient Cu NP loading is achieved with the Ag-seeding as compared to Pd-seeding for the case of full conformal copper NP films.

EXPERIMENTAL SECTION

ELECTROSPINNING

PAN powders (Sigma-Aldrich, M_w=150000 g/mol, ρ = 1.18 g/cm^3) were dissolved in dimethylformamide, DMF, to make a solution with 13 wt% PAN concentration. Subsequently, 1 wt% acetone was added to the resulting solution. Acetone has been shown to mitigate or eliminate bead formation in the electrospinning process [27]**.** The solution was stirred continuously for 24hrs at room temperature. The electrospinning solution was loaded into a 3mL syringe with a 19ga (ID = 0.8126 mm) needle. The collector plate was aluminum foil situated at a distance of 15cm from the syringe tip. A voltage generator (Model SL300, Spellman NY) supplied a constant DC voltage of 15 kV between the collector plate and needle

tip, creating an electric field strength of 100 kV/m. Flow rate was maintained at 0.34 mL/hr by a syringe pump (Advance infusion pump series 1200). Total collection time was 8 hours. Finally, the non-woven mats were peeled off from the aluminum substrate, resulting in a mat with a nominal thickness of 30 μm and a total planar dimension of 13 cm x 13 cm.

Silver Seeding of PAN fibers

Rectangular coupons with dimension 15 x 30 mm^2 were cut from the mat for deposition. To improve handling, ensure planar configuration during immersion in the various baths and mitigate the collapsing effect of surface tension of the aqueous solution after bath emersion, fiber mats were affixed to strips of carbon adhesive tapes. A schematic of the deposition process is shown in figure 1.The fiber mats were treated in a 1.63 M solution of sodium carbonate (Na_2CO_3) for 3 min. Next, Alkaline hydrolysis of the samples was achieved in 1 M solution of sodium hydroxide (NaOH) at a temperature between 45 – 50°C for 15 min. For the seeding, two different concentrations of silver precursor ($AgNO_3$), 0.1 M and 0.01 M, were systematically investigated. A 10 ml solution of both salt concentrations was prepared: to each bath, 200 μl of ammonia solution (NH_4OH) was first added under constant stirring, causing the transient appearance of a brownish color in the original clear solution for the bath with concentrations of 0.1 M $AgNO_3$, and no perceptible color changes for 0.01 M $AgNO_3$ concentrations.

Lastly, a 5 ml solution containing 10 wt% glucose was added to the solution and stirred for 1 minute. Thereafter, samples were immersed in the silver baths for 1 minute, and then rinsed thoroughly. A progressive brownish yellow discoloration of the sample was observed during immersion in the 0.1 M $AgNO_3$ baths, while samples in the 0.01 M $AgNO_3$ bath seemingly maintained the white color of the PAN fibers but acquired a very slight yellow hue after rinsing and drying. All seeding baths were operated at room temperature under quiescent conditions. A fresh silver bath was prepared for each sample. The reaction pathway has been suggested to proceed as follows [28]:

$$Ag^{+}{}_{(aq)} + 2NH_{3\,(aq)} \rightleftharpoons Ag(NH_3)_2^{+}{}_{(aq)} \quad (1)$$

$$2[Ag(NH_3)_2]^+ + R-CHO\ (glucose) + H_2O \rightleftharpoons 2Ag^0{}_{(s)}(seeds) + 2NH_3 + R-COOH + 2H^+ \quad (2)$$

In this scheme, the silver ions react with NH_3 to form a two-coordinate ammine complex as in reaction (1), manifesting experimentally as the aforementioned brownish color change. These species are subsequently reduced by glucose to silver seeds, reaction 2.

Figure 1: Schematic of the palladium and silver seeding processes on electrospun PAN fibers for electroless copper deposition, colors of solutions roughly denote actual visible color changes during processing.

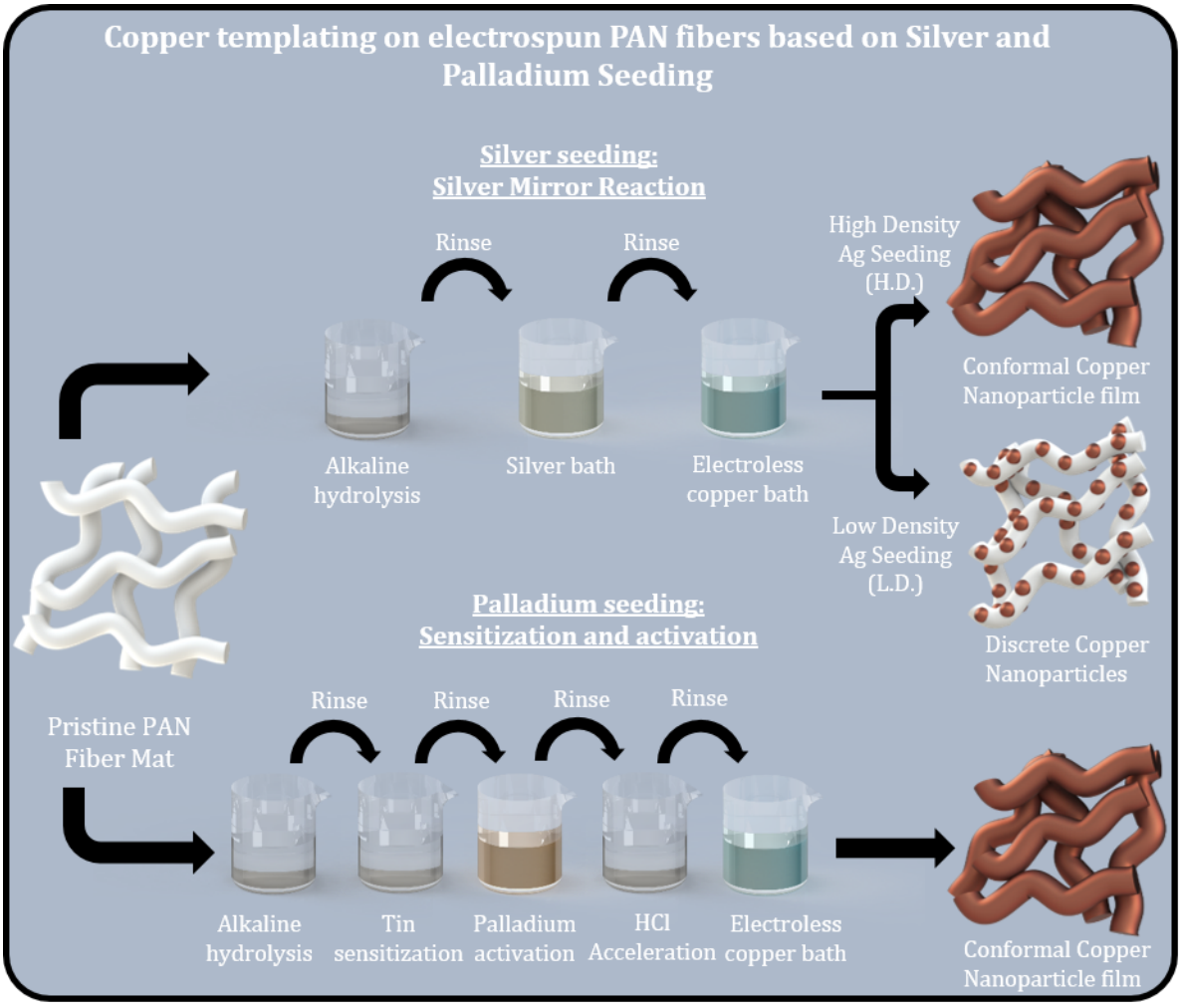

Palladium seeding: Two step activation protocol

The two-step activation protocol was preceded by sample pre-cleaning and alkaline hydrolysis procedures noted in the previous section. The sensitization bath was a mixture of 5g of $SnCl_2.2H_2O$, 8 ml of HCl (AR 37%) and 40ml of deionized water, and the activation bath was 0.1 g of $PdCl_2$, 5 ml of HCl (AR 37%) and 20 ml of water. In preparing these solutions, both metal salts were first dissolved in the stated volumes of hydrochloric acid under mild stirring. For the sensitization solution, the stated volume of deionized water was added after the mixture of the tin chloride and hydrochloric acid became transparent, signifying complete dissolution. For the activation solution, addition of deionized water occurred after a brownish turbid bath was observed. The mats were sequentially immersed in these baths for three minutes each. After the activation step, the mats acquired a greenish coloration that gradually turned milky brown upon extended rinsing. Prior to immersion in the electroless copper bath, the fiber mats were treated in an acceleration bath consisting of 1M HCl for 3 minutes; this step aids the dissolution of excess tin or tin chlorohydroxide from the surface [29]. Mats were rinsed between each step, and the bath operating conditions were similar to silver seeding processes. Also, a fresh bath was prepared for each sample. The electrochemical reaction pathway is one of galvanic displacement, wherein the tin ions adsorbed on the fiber surface reduce palladium ions to the metal on introduction in the activation bath, and are subsequently replaced by them [30]

$$Pd^{2+} + Sn^{2+} \rightarrow Sn^{4+} + Pd^{0} \quad (3)$$

Electroless Copper Deposition

An initial solution containing 0.1g of copper salt ($CuSO_4.5H_20$), 0.6g of disodium ethylene diamine tetraacetate (Na_2H_2EDTA) and 20 ml of deionized water was prepared. Subsequently, 280 µl of formaldehyde (HCHO), the reducing agent, was added into the solution. Sodium hydroxide droplets from a 1.15 M solution were pipetted into the solution to adjust the pH of the metastable bath to 12.3-12.4, measured using a pH meter (AB15, Thermo fisher scientific). A simplified scheme for the anodic and cathodic half reactions as well as overall the electrochemical reaction for which formaldehyde (HCHO) is the main reducing agent is expressed as [30]:

$$Cu^{2+} + 2e \longrightarrow Cu \quad (4)$$

$$HCHO + 2OH^- \longrightarrow HCOO^- + H_2O + \frac{1}{2}H_2O + e \quad (5)$$

$$Cu^{2+} + 2HCHO + 4OH^- \longrightarrow Cu + 2HCOO^- + 2H_2O + H_2 \quad (6)$$

It is noteworthy that formaldehyde is susceptible to disproportionation reactions that give rise to the formation of formic acid and methanol, and the rate of this reaction increases with increasing pH [30]. This may potentially reduce the rate of precipitation in the electroless copper bath [24]. Both silver and palladium seeded fibers were immersed for 5, 10 and 15 minutes respectively i.e. evolution of copper nanoparticles was time-resolved. In general, the bath color change sequence was from clear blue to pale green and lastly deep green with evident turbidity signifying homogenous precipitation. However, this color change sequence proceeded in a much rapid manner in the case of the Pd-seeded fibers as compared to the Ag-seeded fibers, accompanied by a bulk solution precipitation of Cu NPs. Afterwards, samples were rinsed in deionized water and air-dried. Henceforth, Cu-deposited seeded fibers will be named following this format: PAN-X-Cu-Y; where X is the seed catalyst and Y denotes immersion time.

Characterization

Scanning electron microscopy was carried out on an FEI Nova NanoSEM operated in secondary electron mode. All samples were sputter-coated with a thin layer platinum using a Cressington (208HR) sputter coater at a plasma current of 40 mA for 60 s. Image processing was done using ImageJ (National Institute of Health, MD, USA). Transmission electron microscopy (TEM) images were obtained for ultramicrotomed cross-sections using a FEI Tecnai G2 20. For ultramicrotomy, samples were sawed from epoxy embedding blocks and mounted in a universal specimen holder from an Ultracut E ultramicrotome (Leica Microsystems, Vienna, Austria). Samples were trimmed with a razor blade and faced on a routine diamond knife to 1mm squared block faces. Ultrathin sections were prepared at 90 nm thickness (a pale gold color) with a 45° diatome diamond knife with a 6° clearance angle. Thin sections were prepared with a cutting speed of 1 mm/s and floated on water. Individual sections were collected with a diatome perfect loop on 100 mesh formvar carbon coated grids. X-ray diffraction spectra was obtained using a Bruker D8 focus system operating in the bragg-brentano geometry at 40 kV and 40mA. Scan speed was 1°/min, spanning a range of 2Θ angles from 10° to 75°. Crystallite size, L, was calculated from the x-ray data using the Debye-Scherrer equation:

$$L = \frac{k\lambda}{\beta cos\theta} \quad (7)$$

where $k = 0.90$, $\lambda = 0.154$ nm (Cu Kα radiation), β is the full width at half maximum of the (111) reflections and θ is the Bragg angle.

Raman shifts were collected using a Renishaw inVia Raman microscope with a 532 nm laser (at 1% power) with a grating of 2400 L/mm and an objective lens of 100x. ATR - FTIR was performed using a PerkinElmer IR 100 spectrometer operated in transmittance mode. Thermal decomposition and relative composition analyses of the metallized PAN fibers were carried out using a TGA Q50 TA instruments (TA instruments, DE, USA). Samples were loaded in a platinum pan, and heated in a nitrogen atmosphere at a constant ramp rate of 10° C/min from room temperature to 800°C

RESULT AND DISCUSSION

An intricate interplay of electrostatic fields, polymer rheology, solution dielectric properties and surface phenomena, electrospinning provides a facile technique for the production of submicron to micron sized fibers. In brief, semi-continuous polymer jets are electrostatically drawn from the needle tip, developing a series of in-flight bending and whipping instabilities [31, 32] that successively create thinner jet cross-sections until they impinge on the collector plate as solid fibers after solvent evaporation. Figure 2a shows the random, layered arrangement of the as-spun PAN fibers exhibiting complex topology. The fibers had uniform cross-sections with an average diameter of 1.017 ± 0.08 μm. Furthermore, the individual fiber surfaces were relatively smooth, figure 2b, exhibiting slight surface asperities that could be attributed to artifacts of the rapid in-flight solvent evaporation.

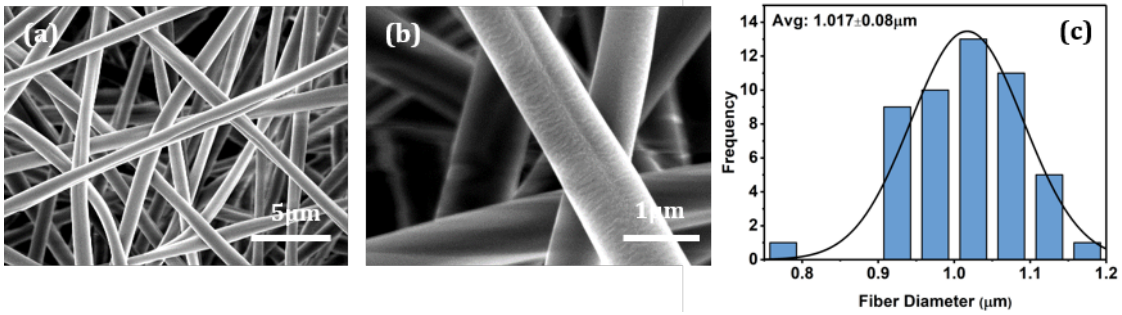

Figure 2: SEM micrograph showing: (a) as-spun PAN fibers (b) Surface topography of Individual fiber. (c) Histogram of fiber diameter distribution. Average fiber diameter is 1.017 ± 0.08 μm.

Silver ions are firstly chelated in the silver mirror reaction, and subsequently reduced to silver atoms/seeds, whereas the direct reduction of palladium ions to palladium atoms/seeds is the major electrochemical reaction in the two-step process. In the presence of the PAN fibers, these redox reactions take place preferentially on the fiber surface. Importantly, by virtue of the mat wicking resulting from capillary effects, the working solution is able to reasonably penetrate the complex mat architecture presented by tortuous fibers and random layering. Figure 3 shows the microstructure of the seeded fibers. A discrete distribution of deposited seeds is evident for both Ag seeding protocols, figure 3a and b, as well as for Pd seeding, figure 3c. This system of seed distribution is the consequence of the combined effects of surface sites amenable to nucleation and their stochastic bifurcation into cathodic and anodic sites as is characteristic of electroless processes [20]. All seed morphologies approximate a spherical shape. However, for Ag seeding, a marked difference in seed density is observed: for the fibers immersed in SMR bath with 0.1 M $AgNO_3$, a high density of fine Ag seeds in close proximity can be observed; while, fibers treated in SMR bath with 0.01 M $AgNO_3$ showed comparatively finer Ag seeds that are sparsely distributed, leaving much of the fiber surface exposed. Furthermore, apparent seed density increases from 23 ± 10 particles/μm^2 to 47 ± 6 particles/μm^2, and particle size increased from 29 ± 7 nm to 60 ± 18 nm with increase in the concentration of the silver salt in the SMR bath. In essence, modulating the silver precursor concentration, while keeping invariant the chelation and reducing agent concentration, leads to fewer apparent nucleation and a smaller seed size on the PAN fiber surface. Henceforth, Ag-seeded samples will be referred to as (H.D.) and (L.D.) for the high and low seed density cases respectively. It can also be deduced that the incubation time is independent of the seeding density.

On the other hand, the Pd seed crystals were ultra – fine, having an average particle size of 5.6 nm (determined from XRD patterns, under the assumption that the crystallite size ≈ particle size). This ultra-fine nature precluded a quantification of the apparent Pd seeding density, but it is qualitatively estimated to be in excess of seed densities of the Ag-seeded fibers. This is in accordance with general observations of Pd seed densities on tin–sensitized planar substrates [33]. In the two – step activation procedure, hydrochloric acid in the sensitization bath inhibits the hydrolysis of tin (II) chloride into insoluble hydroxotin (II) chloride (Sn(OH)Cl), facilitating the formation of tin chloro – complexes that have been posited as the active reducing species [34]. Consequently, the hydrochloric acid concentration strongly modulates the evolution of catalytic palladium seeds upon activation, controlling particle size and promoting high seeding densities [33]. For instance, for sensitization baths with 30 mL/L and 60 mL/L of HCl, Pd seeding densities of 640 and 1910 particles/μm^2 were observed respectively on planar TiN [35]. In this work, the HCl concentration in the sensitization bath was 200 mL/L, and it can be inferred that the Pd seeding density will be correspondingly high.

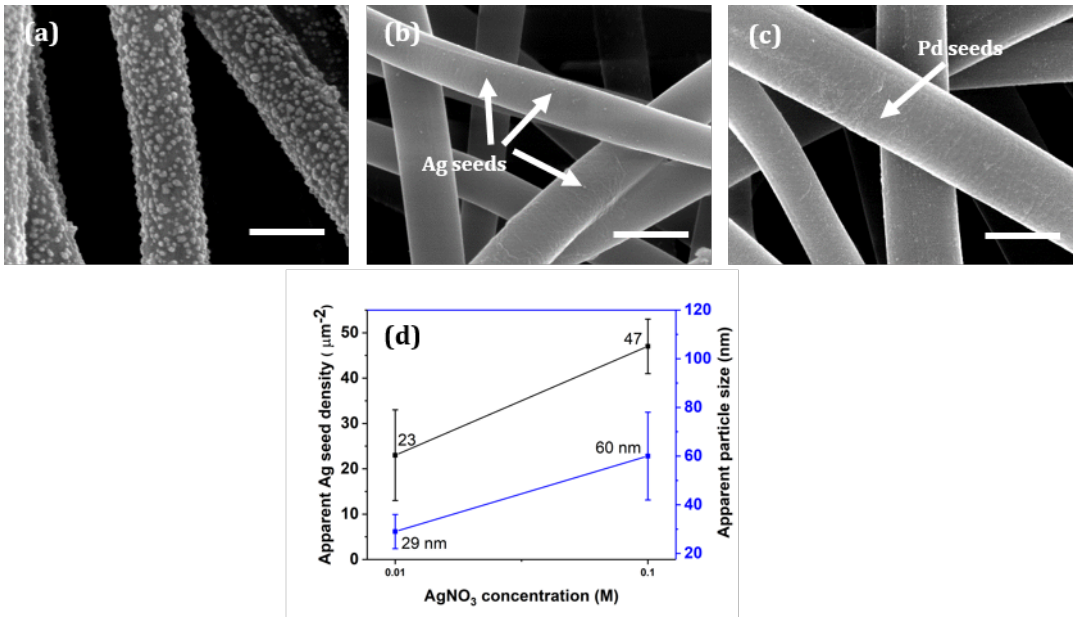

Figure 3: SEM micrographs of (a) High density Ag-seeding obtained from 0.1 M $AgNO_3$ in S.M.R bath (b)) Low density Ag-seeding obtained from 0.01 M $AgNO_3$ in S.M.R bath (c) fine palladium particles on the surface of the PAN fibers (d) Ag seeding density and particle size versus $AgNO_3$ concentration in S.M.R bath. Scale bar is 1 μm

The reaction pathway for the activation of formaldehyde (HCHO) in an electroless copper deposition process has been studied in detail [36]. In essence, formaldehyde is hydrolyzed to methylene glycol ($H_2C(OH)_2$, but it takes the methyl diol anion form, $H_2C(OH)O^-$, due to the high pH of the electroless copper solution. The negative charge of this molecule lowers the thermodynamic barrier to the abstraction of hydrogen from the carbon atom (in the C – H bond) necessary for initiation of the anodic oxidation process, equation (5). The dehydrogenated product is terminally oxidized to formic acid (or formate anions in an alkaline bath) with a corresponding reduction of copper species. Analogously, as has been shown with saturated hydrocarbons, transition metals possess unique chemistries that facilitate the breakage of the C – H bond required for dehydrogenation [37]: in close proximity, the antibonding molecular orbital, σ^*_{C-H} is populated by electrons from the occupied transition metal d orbital, inducing a weakening of these bonds; at the same time, metal – H interaction/bonding occurs with an attendant overlap of electron population. Based on these processes, Pd and Ag seed crystals facilitate the dehydrogenation of formaldehyde, allowing the nucleation and subsequent growth of copper nanoparticles on the surface of the electrospun PAN fibers. As an advantage, deposition is not terminated when these seed crystals are expectedly occluded by deposited copper species given that Cu^0 also represents adsorption sites for methyl diol anion activation and oxidation [36]. This affords easy control over copper growth during deposition on the PAN fibers.

Figure 4 shows the evolution of copper nanoparticles on the Ag- and Pd-seeded fibers, and the lower magnification images of deposition can be found in figure S1; for both seeding processes copper coatings can eventually occur. The first observation of note is that both Ag seeding conditions have an incubation time of ≥ 5 min before Cu begins to deposit, since the microstructures after 5 minutes Cu deposition, fig 4a and g, are qualitatively similar to that of their corresponding Ag-seeded fibers, figure 3a and b. This delayed deposition of Cu on the Ag seed systems is likely due to time needed for the spontaneous polarization of the equilibrium potentials of the redox half reactions (reactions 4 & 5) to establish a compromise potential at which metal deposition takes place according to the mixed potential theory [20]. As an example, literature reports of an electroless copper bath that consists of formaldehyde (HCHO) as reducing agent and ethylenediamminetetraacetic acid (EDTA) as complexing agent have shown that the mixed potential is reached only after about 4 minutes (on Cu substrates at a pH of 12.5) of exposure to the plating solution [20]. Secondly, for high-density Ag-seeded fibers, as the deposition time increases, a progressive increase in Cu coverage from distinct

particles/islands to full consolidated films is observed. At ten minutes deposition, PAN fibers were substantially covered with contiguous copper nodules, but distinct patches of the underlying surface are still visible; a fully conformal Cu NP film on the fibers is not evident until 15 minutes deposition, with the sporadic occurrence of copper outgrowths, fig 4c. The hierarchical assembly of Cu NPs is clearly evident: at 10 minutes deposition, single Cu NPs aggregate into clusters of irregularly shaped nodules on a PAN fiber core.

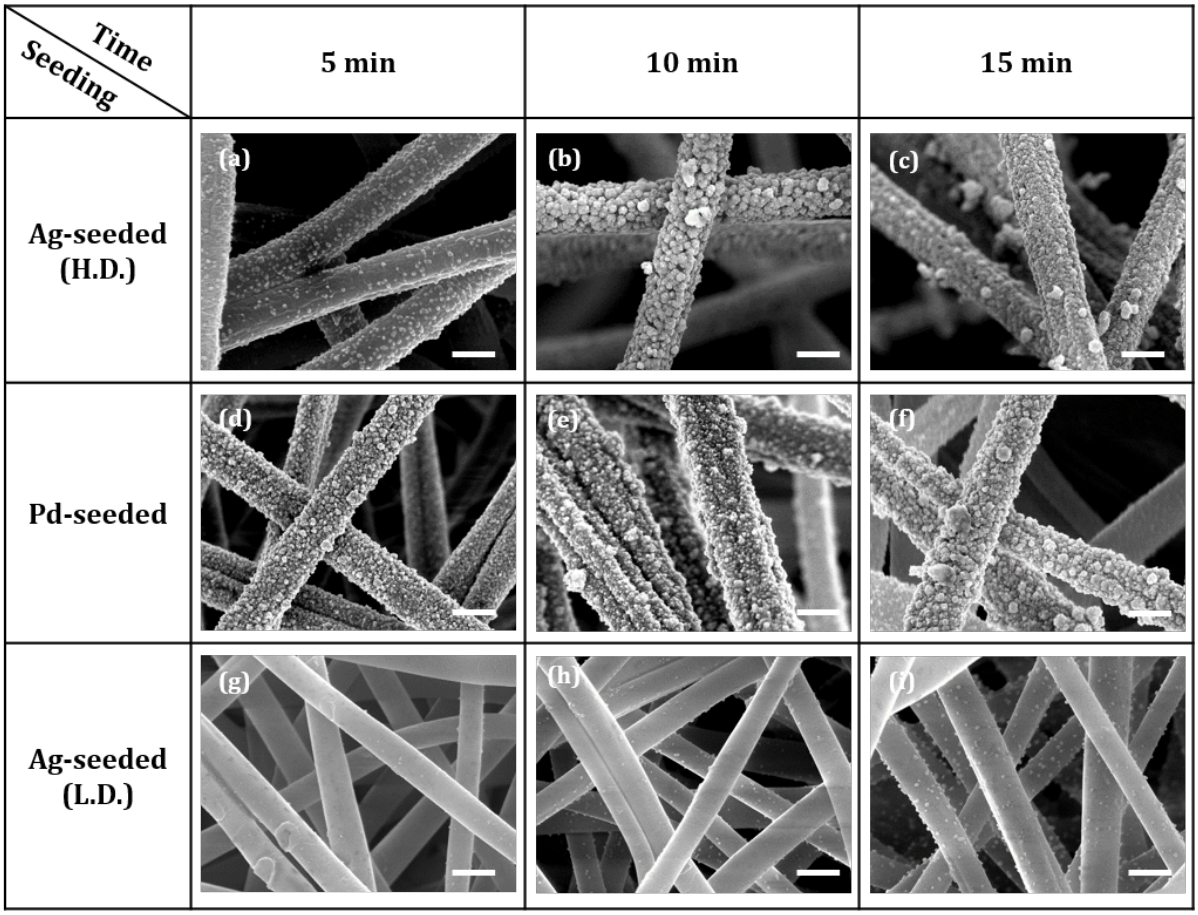

Figure 4. Evolution of copper nanoparticles on the seeded fibers. SEM micrographs for: (a) PAN-Ag-Cu-5 (b) PAN-Ag-Cu-10 (c) PAN-Ag-Cu-15 for High density seeding; (d) PAN-Pd-Cu-5 (e) PAN-Pd-Cu-10 (f) PAN-Pd-Cu-15 for Pd seeding. (g) PAN-Ag-Cu-5 (h) PAN-Ag-Cu-10 (i) PAN-Ag-Cu-15 for low density seeding. Scale bar is 1 µm

This subsequently transforms into full conformal and compact copper nanoparticle coatings at 15 minutes deposition, Figure 4c. Moreover, the copper nanoparticle films contained intermittent voids or mesopores. One plausible conjecture is that the voids may be attributed to

hydrogen gas evolution as predicted by equation (6), which effectively acts as a barrier to densification in the deposition field. A more probable explanation may be that voids form as a result of geometric misfit between adjacent particles, large enough to be uncovered during the particle/nodule growth process [30].

The low density Ag-seeded samples maintain a discrete distribution of copper islands on the PAN fibers after 15 minutes of exposure to the copper electroless plating solution. The island size increased from 44 ± 16 nm at 10 minute deposition to 82 ± 23 nm at 15 minute deposition, but has still not formed a compact film. Since the initial particle density was 29 μm^{-2} (and average particle spacing of ≈ 210 nm, for particle size of 29 nm) more time will be needed to create a compact film. Coverage is modulated by the density of catalytic silver seeds, with the Cu NPs growing exclusively on the silver core seeds, and large areas of the fiber surface are devoid of copper NPs. In addition, copper NP growth evolved to conform to the spherical morphology of the underlying Ag seeds.

The microstructural evolution of Cu NPs on Pd-seeded fibers are shown in figure 4d-f. In contrast to the Ag-seeded fibers, a near-complete copper coverage is observed after 5 minutes deposition, signifying that the mixed potential is attained rapidly on Pd seed systems, and this enhances the kinetics of precipitation, at least before occlusion of the seeds by the first few monolayers of Cu. Thus, with the palladium seeds, the incubation time is << 5 min. This is a similar observation as previous studies of the nascent stage of growth of copper nanostructures on palladium-seeded TaN substrates (seed size, 5 – 10 nm), that showed that continuous copper coverage was obtained after deposition times of 45 s – 1 min [38, 39]. The shorter incubation time may be explained in terms of the three orders of magnitude difference in measured exchange current densities for H_2 evolution on palladium with respect to silver: this value, which is 1.3×10^{-6} A/cm^2 for silver, and 1×10^{-3} A/cm^2 for palladium [21], will, in principle, correlate with the rate of the aforementioned dehydrogenation process, and is a function of the relatively weaker binding of hydrogen with silver in contrast to palladium (in the classic volcano plots of current density vs free energy of hydrogen adsorption, palladium situates close to the peak, and silver lies close to the lower right leg [40]). The deposit microstructures are qualitatively similar with increasing deposition time, with greater copper outgrowth at 10 min and 15 min, figure 4e and f. The copper nodules on the Pd seeded fibers were much finer than those observed on the high density Ag seeded fibers, and they aggregated into a rocklike, porous film structure. The finer nodules are likely a result of the comparatively higher density of Pd seeds, providing a greater number of nucleation centers that presumably confer a

diffusion-dominated growth process for the copper nodules. So, in summary, the Pd seeded fibers exhibit a higher seeding density and a lower incubation time, leading to the more rapid formation of a compact Cu coating.

Figure 5 shows, in greater detail, the resultant microstructures for the three distinct seeding regimens after 15 minute Cu NP deposition. In particular, the comparison between conformal copper nanoparticle films obtained from Ag-seeding (H.D.) and Pd-seeding, figure 5a and b, shows apparent differences in film compactness.

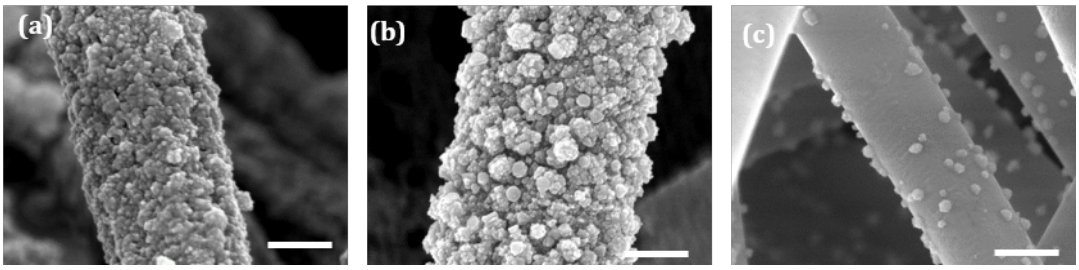

Figure 5. High magnification microstructures of copper evolution for (a) PAN-Ag-Cu-15 (H.D.) (b) PAN-Pd-Cu-15 (c) PAN-Ag-Cu-15 (L.D.). Scale bar is 500 nm

This indicates that hydrogen gas evolution is substantially greater for Pd-seeded fibers, at least in the early stages of deposition. The enhanced H_2 "bubbles" formation creates void-filled deposits that serve as the "irregular" templates for subsequent deposition as will be shown more clearly by cross-sectional TEM images. Accordingly, it is expected that the observed roughness should confer an increased surface area. For the low-density Ag-seeding, the nanoparticle islands are non-faceted, suggesting, on the overall, that the deposition process is faster than surface diffusion.

Figure 6 shows TEM images of representative cross-sections of PAN-Ag, PAN-Pd, PAN-Ag-Cu-15 (H.D.) and PAN-Pd-Cu-15. Generally, the Ag- and Pd- seed crystals as well as deposited Cu NPs conform to the substrate geometry, and deposition/precipitation events are restricted to the PAN fiber surface. The cross-sections are consistent with their corresponding SEM images in figures 3, 4, and 5 respectively. However, for PAN-Ag, figure 6a1, finer Ag crystals on the order of 3 – 4 nm are interspersed between the island particles, previously unobservable in the SEM image of figure 3a. Although the majority of Pd seeds were bound to the fiber surface in the PAN-Pd samples, varying degrees of particle embedding (a few nm beneath the fibers surface) was observed. The reason is not clear yet, but the shearing force of the diamond

knife may inadvertently displace the Pd seeds. The PAN-Pd-Cu-15 samples, figure 6b2, do not exhibit such embedding. The distinction in the copper nanoparticle film growth as facilitated by Ag seeding and Pd seeding is clearly observed in figure 6a2 and b2 respectively: the PAN-Ag-Cu-15 (H.D.) exhibited a highly compact film structure as is evidenced by the greater mass thickness contrast; on the other hand, PAN-Pd-Cu-15 exhibited loosely packed film deposits with attendant microporosity from inclusion of H_2 bubbles as discussed previously. Corresponding latitudinal cross-sections for PAN-Ag-Cu-15 (H.D.) and PAN-Pd-Cu-15 are shown in figure 6a3 and b3 respectively,

Figure 6. Bright Field TEM images of (a1 Latitudinal cross section of PAN-Ag (a2) Latitudinal cross-section of PAN-Ag-Cu-15 (a3) longitudinal cross-section of PAN-Ag-Cu-15 (b1) Latitudinal cross-section of PAN-Pd (b2) Latitudinal cross-section of PAN-Pd-Cu-15 (b3) longitudinal cross-section of PAN-Pd-Cu-15. Scale bars are 200 nm

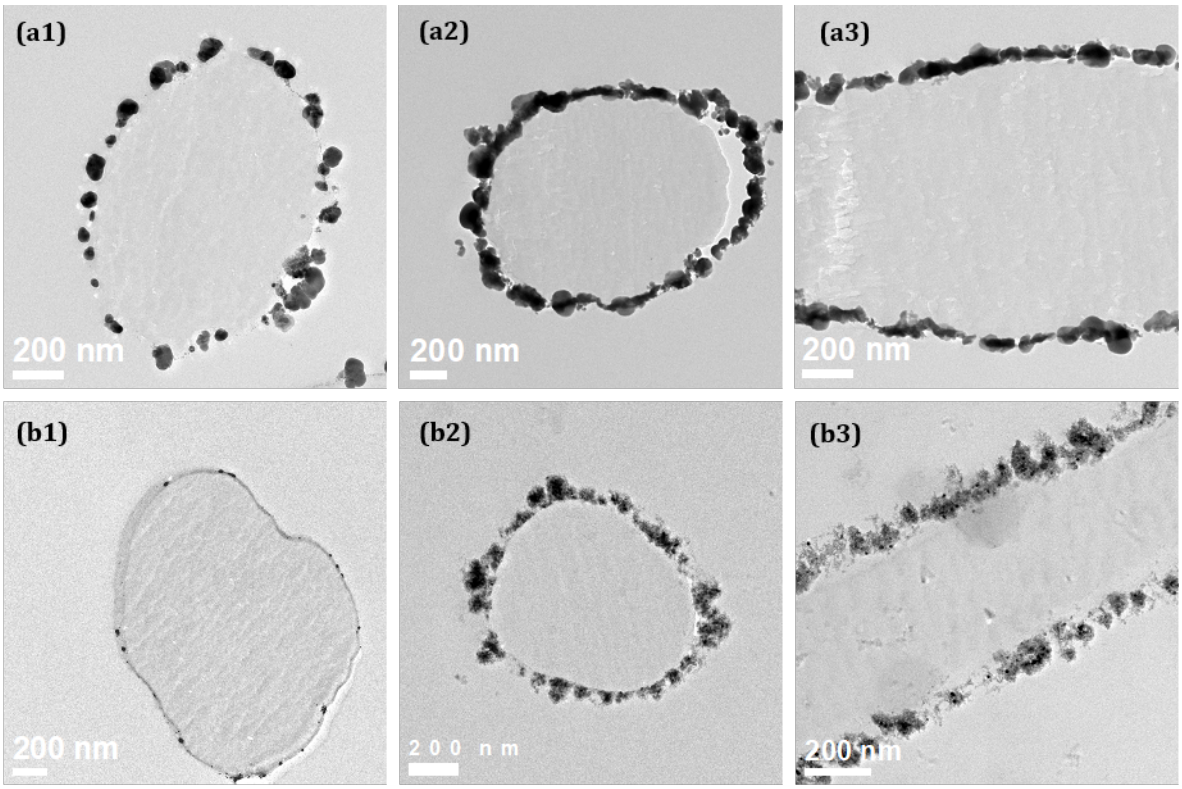

Phase confirmation and crystallite size measurements of the metallized fibers were evaluated using x-ray diffraction. Figure 7 shows the obtained diffraction patterns of the H.D. Ag-seeded fibers and Pd-seeded fibers, wherein the patterns can be viewed as a superimposition of the individual patterns of PAN and the grown metallic species. For all seeding protocols, peak broadness is indicative of the nanoparticulate nature of the deposited metallic species. The

broad peak between 20° and 35° can be attributed to the attendant amorphicity of the electrospun PAN fibers. For the H.D. Ag seeding, figure 7a, the presence of silver crystals in the seeded fibers is evidenced by characteristic silver peaks at Bragg angles of 38.4°, 44.3° and 64.5° which correspond to the {111}, {200}, and {220} Ag planes respectively (JCPDS Card No. 4-783). For the Pd-seeded fibers, figure 7b, characteristic Pd peaks are observed at 40.1° and 46.2° for {111} and {200} Pd planes respectively (JCPDS Card No. 46-1043). However, there were apparent differences in the intensity of the {111} reflections despite identical seeding and measurement conditions. This could be a result of sample and measurement variability with respect to possible differences in fiber mat packing, slight differences in probe volumes etc.

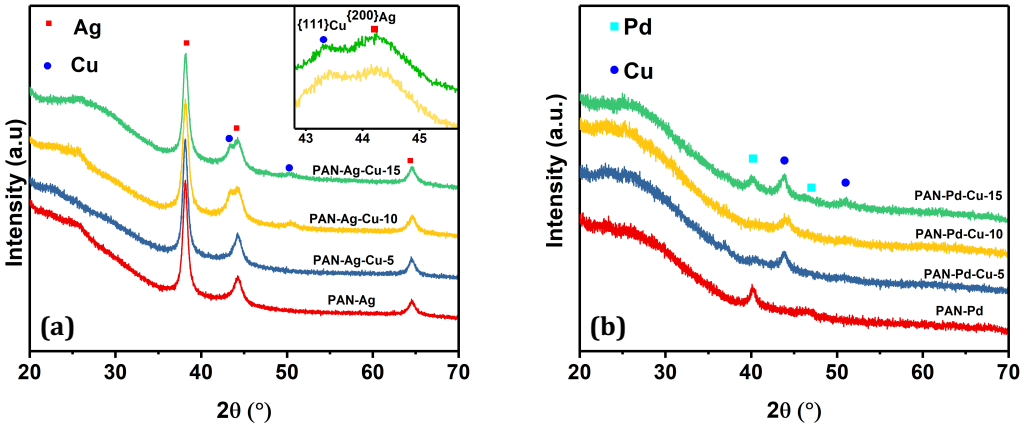

Importantly, copper peaks at 43.5° and 50.4° for (111) and (200) Cu planes (JCPDS Card No. 4-0836) became apparent at high deposition times i.e. at 10 minutes and 15 minutes for H.D. Ag-seeded fibers, and at 5 min onwards for the Pd-seeded fibers, corroborating the microstructural observation of a marked distinction in induction/incubation period for copper deposition for both seeding systems. In addition, for Ag-seeding, the evolution of copper peaks at 10 minutes is consistent with observations made with dynamic light scattering of time-resolved aqueous solution precipitation of Cu NPs catalyzed by Ag NPs [41]. In accordance with the attenuation of the overall intensity of silver and copper reflections for L.D. seeded fibers, the higher index reflections were either obscured by background signals or absent, shown in figure S2. Average silver crystallite size was 12.75 nm and 4.51 nm for H.D and L.D.

Ag seeding respectively, signifying that the Ag particles in figure 3 are polycrystalline in nature. For both seeding chemistries, the average size of the Cu NPs is ~9 nm.

Raman Spectroscopy

Considering the imbuement of the electrospun mats with the active species of the seeding and electroless copper deposition processes, structural modification of the underlying PAN fiber is expected. Raman spectroscopy provides structural characterization of carbonaceous materials [42]. Complete Raman shifts for the three distinct seeding regimen and attendant time-resolved copper NP evolution is shown in figure S3. The shifts can be split in two distinct regions [43]: a first order region which spans shifts between 1100-1800 cm^{-1} and the second order region from 2200-3400 cm^{-1}. The pristine fibers show a narrow, sharp peak in the second order region at 2240 cm^{-1}, characteristic of the cyano- functional group present in polyacrylonitrile – which is also an infrared (IR) active band, figure S4 – and a second-order band at 2932 cm^{-1}. Incipient, convolved high frequency bands at 1350cm^{-1} and 1580cm^{-1} respectively classified as the D and G bands are observed in the seeded fibers i.e. PAN-Ag (H.D.) PAN-Ag (L.D.) and PAN-Pd, figure S3a-c. Upon copper NP deposition, the relative intensities of these bands became more distinctive with increasing deposition times, more so for the Pd-seeded fibers, figure S3c. While the observed evolution of these specific peaks are undoubtedly a result of chemical modifications, it is also important to note that localized plasmon resonances of the copper NPs upon laser excitation enhances Raman scattering [44]. Furthermore, it is established that metallic nanoparticle density as well as inter-particle spacing both augment this enhancement [45]. Hence, we make definitive comparisons of surface chemistry modifications using sample instances that have high copper nanoparticle density and distinguishable D and G bands, which correspond to samples with 15 min immersion times. The acquired Raman shifts for pristine PAN, PAN-Ag-Cu-15 (H.D.), PAN-Ag-Cu-15 (L.D.) and PAN-Pd-Cu-15 shown in figure 8a.

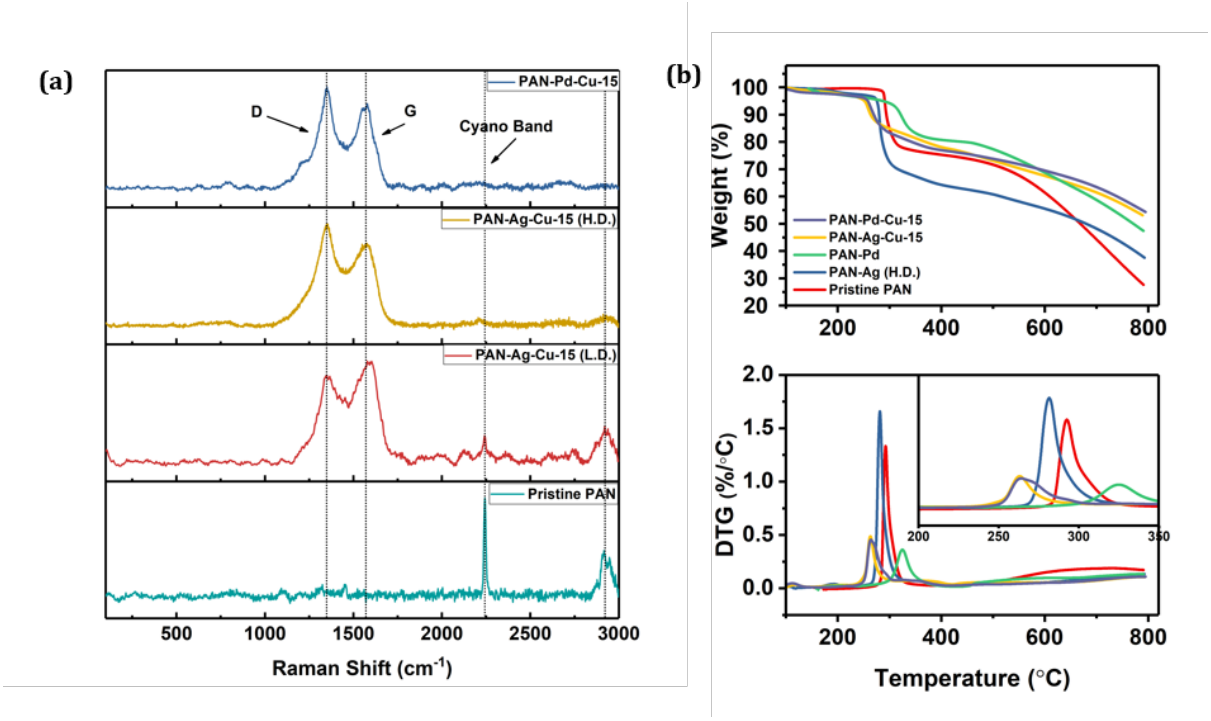

Figure 8: (a) Raman shifts for pristine PAN, PAN-Ag-Cu-15 (L.D.), PAN-Ag-Cu-15 (H.D.), PAN-Pd-Cu-15 (b) Decomposition profile of the metallized PAN fibers for TGA analysis (top); Derivative curves with (bottom), inset plot highlights the relative shifts in temperatures at maximum weight loss for the samples

The G-band originates from "in-plane" E_{2g} type vibrational mode of overlapping sp^2 – hybridized carbon atoms, while the D-band or defect band is an "out-of-plane" A_{1g} type vibrational mode generated by structural disorder or introduction of heteroatoms in the carbon-based structure [43, 46]. Also, the D band has been attributed to the breathing mode of sp^2 atoms in ringed structures [47]. In the context of PAN metallization, both bands are indicative of the possible cyclization of PAN molecules i.e. the transformation of distinct -C≡N groups into conjugated systems of C = N bonds, forming a part of connected six-membered cyclical structures [48]. FTIR spectra in figure S4 provides added evidence of this transformation. However, cyclization does not extend into the bulk of the PAN fibers, given that the cyano-bands are still visible in the infrared spectra of these samples (Given a PAN refractive index of 1.5, for a mid–IR incident probe wavelength of 2240 cm^{-1}, the theoretical penetration depth is ~ 0.90 μm which is on the order of the fiber diameter). Additionally, the evidence of surface chain cyclization is further strengthened by observing the manner of evolution of the D and G bands in relation to the cyano band: a marked attenuation of the cyano band intensity is apparent

in the Raman shifts of PAN-Ag-Cu-15 (H.D.), PAN-Ag-Cu-15 (L.D.) and PAN-Pd-Cu-15 in figure 8a (also observed in figure S3a–c), and this is accompanied by the appearance of D and G-bands, suggesting that the depletion (or more appropriately, conversion) of the cyano-functional group on the surface of the fiber and emergence of aromatized components may be closely related. In parallel, the band intensity at 2932 cm^{-1}, attributable to methylene stretching, is observed to be dramatically reduced for PAN-Ag-Cu-15 (H.D.) and PAN-Pd-Cu-15 samples. A commonly used metric for quantification of the degree of structural organization/disorganization is ratio of intensities of the D and G bands (I_D/I_G). As disorganization increases, the ratio increases and vice versa [43]. For PAN-Ag-Cu-15 (H.D.), PAN-Ag-Cu-15 (L.D.) and PAN-Pd-Cu-15, I_D/I_G are 1.25, 0.86 and 1.16 respectively. Accordingly, the order of decreasing disorganization is PAN-Ag-Cu-15 (H.D.) > PAN-Pd-Cu-15 > PAN-Ag-Cu-15 (L.D.). Broadly, these ratios allow the inference of a high degree of surface disorganization (better termed as a reorganization with respect to this study) of the PAN fibers, and are roughly proportional to the seeding densities (and attendant Cu NP coverage) in the respective nanocomposite systems

Thermogravimetric analysis

Thermograms and DTG curves from the controlled pyrolysis of pure PAN, PAN-Ag-Cu-15 (H.D.), PAN-Ag (H.D.), PAN-Pd and PAN-Pd-Cu-15 are shown in figure 8b. In general, thermal decomposition of the samples proceeded in a multi-step manner. Furthermore, weight loss regimes can be grouped under three broad temperature ranges: from room till about 250°C, slight weight losses are observed, attributable to the emission of water molecules and other volatile products [49]; dramatic weight loss from 250°C - 330°C is commonly observed in PAN-containing materials, and is a result of evolution of ammonia gas and hydrogen cyanide accompanied by a thermally induced cyclization of the nitrile groups; the gradual weight loss between 330°C - 800°C has been attributed to methane and hydrogen gas emissions [50]. However, the chemical treatment processes may presumably alter slightly the constitution of these classic pyrolytic PAN products. Importantly, a degradation in the thermal stability of PAN-Ag-Cu-15 (H.D.), PAN-Ag (H.D.), PAN and PAN-Pd-Cu-15 is observed in the DTG curves, figure 8b, wherein the differential in temperatures at maximum weight loss (peak temperatures) of these samples with respect to the pure PAN fibers was between 12°C - 30°C. The values are shown in table 1. While the cyclization of the nitrile functional groups as

evidenced by the Raman spectra in figure 8, has been postulated to enhance the thermal stability of PAN [51], this effect may be nullified and reversed by the exceptional thermal conductivity/transport of the copper and silver nanoparticle films through an enhanced thermal coupling to the underlying PAN fibers during pyrolysis that manifests as a thermal stability degradation. This observation is in contrast to improvements in thermal stability of PAN fiber nanocomposites where the metallic nanoparticles are dispersed in the fiber matrix [52, 53]. However, PAN-Pd sample exhibited an enhanced thermal stability and this may be attributed to the size-mediated degradation of the thermal conductivity of metallic nanoparticles which occurs when the characteristic dimensions of the body approaches the mean free path of conducting electrons [54]. In this case, the Pd particle size (~ 5.6 nm) is much smaller than the typical mean free paths of metallic materials (on the order of tens of nanometers)[54]; coupling this effect with the discrete nature of Pd seed distribution (figure 3c and figure 6(b1)) may induce a less thermally responsive PAN fiber nanocomposite. A summary of the relative composition derived from analysis of the residual char is shown in table 1.

Table 1: Relative composition of the constituent materials in the metallized fibers for PAN-Ag-Cu-15 (H.D.) and PAN-Pd-Cu-15

Sample	Temp at Max %/°C (°C)	Residual char (Wt %)	Relative composition by weight (%)			
			PAN	Pd	Ag	Cu
PAN	292	28	100	–	–	–
PAN – Ag	280	38	86	–	14	–
PAN – Pd	324	47	74	26	–	–
PAN–Ag–Cu–15 (H.D.)	263	53	65	–	11	24
PAN–Pd–Cu–15	263	54	64	23	–	13

In spite of increased reaction kinetics resulting in very rapid copper deposition from solution as observed previously, the Pd-seeded fibers supported a comparatively smaller amount of copper nanoparticles than the Ag-seeded fibers as seen in Table 1. Again, this stems from the

hydrogen gas/bubble generation that undermines the formation of compact copper nanoparticle films, limiting the amount of material deposited per layer on the PAN fibers.

CONCLUSION

We have made a comparative analysis of electroless deposition of copper nanoparticles on electrospun PAN fibers as mediated by catalytic seeds of palladium and silver to determine conditions that can create continuous conformal copper NP coatings or maintain individually isolated copper nanoparticles. The resultant hierarchical material structures can be used in the fields of catalysis, sensor design, membrane or separation technologies and wound dressing. Cyclization of polyacrylonitrile macromolecules as a consequence of the Pd and Ag seeding and electroless copper metallization processes allow for precipitation/deposition. Each seeding route and chemistry confers distinct features that may be beneficial for some given specific material design requirements. Using the silver mirror reaction for silver seed deposition created a conformal and discrete distribution of copper nanoparticles on the PAN fibers that can be controlled by modulating the concentration of the precursor silver salt, with apparent densities of 23 ± 10 particles/μm^2 and 47 ± 6 particles/μm^2 and corresponding particle sizes of 29 ± 7 nm and 60 ± 18 nm obtained for concentrations of 0.01 M and 0.1 M $AgNO_3$ respectively. The Pd seed size ($\sim$ 5.6 nm) appears to have an even higher density of seeds. The seed density correlates well with the ratio of the D:G band intensities in Raman spectroscopy, implying that cyclization of the surface of the PAN during chemical processing is directly related to the seeding behavior and attendant Cu NP coverage. Time-resolved electroless deposition of copper nanoparticles helped to establish time thresholds or cut-offs for microscopic and diffraction scattering detection of particle formation, being $<<$ 5 minutes on the Pd-seeded fibers and $\geq$ 5 minutes on the Ag- seeded fibers. For the cases of conformal copper nanoparticle coatings, compact films were obtained for the Ag-seeded fibers, whereas for the Pd-seeded fibers the films were porous and rocky with attendant microporosity. TGA analysis showed a degradation in thermal stability of the metallized fibers when the metallic coating size was greater than the electron's mean free path, but a slight enhancement in thermal stability when PAN was coated with isolated Pd particles with a size smaller than the likely mean free path of the eletrons.

ACKNOWLEDGEMENT

This work was funded by the National Science Foundation under grant CMMI 1634772. The Authors will also like to thank Robert Seiler and Shuvo Shoumya of the Life Science Microscopy facility at Purdue University for assistance with T.E.M sample preparation and imaging.

Conflict of Interest

The authors declare that they have no conflict of interest.

References

[1] Sarkar S, Guibal E, Quignard F and SenGupta A 2012 Polymer-supported metals and metal oxide nanoparticles: synthesis, characterization, and applications *An Interdisciplinary Forum for Nanoscale Science and Technology* **14** 1-24

[2] Kaushik A, Khan R, Solanki P R, Pandey P, Alam J, Ahmad S and Malhotra B D 2008 Iron oxide nanoparticles-chitosan composite based glucose biosensor.(Report) *Biosensors and Bioelectronics* **24** 676

[3] Dos Santos D S, Goulet P J G, Pieczonka N P W, Oliveira O N and Aroca R F 2004 Gold nanoparticle embedded, self-sustained chitosan films as substrates for surface-enhanced Raman scattering *Langmuir : the ACS journal of surfaces and colloids* **20** 10273

[4] Bhardwaj N and Kundu S C 2010 Electrospinning: A fascinating fiber fabrication technique *Biotechnology Advances* **28** 325-47

[5] Marx S, Jose M V, Andersen J D and Russell A J 2011 Electrospun gold nanofiber electrodes for biosensors *Biosensors and Bioelectronics* **26** 2981-6

[6] Li X, Wang M, Wang C, Cheng C and Wang X 2014 Facile immobilization of ag nanocluster on nanofibrous membrane for oil/water separation *ACS applied materials & interfaces* **6** 15272

[7] Liu Z, Yan Z, Jia L, Song P, Mei L, Bai L and Liu Y 2017 Gold nanoparticle decorated electrospun nanofibers: A 3D reproducible and sensitive SERS substrate *Applied Surface Science* **403** 29-34

[8] Yadav R and Balasubramanian K 2015 Metallization of electrospun PAN nanofibers via electroless gold plating *RSC Advances* **5** 24990-6

[9] Yu D-G, Zhou J, Chatterton N P, Li Y, Huang J and Wang X 2012 Polyacrylonitrile nanofibers coated with silver nanoparticles using a modified coaxial electrospinning process.(ORIGINAL RESEARCH)(Report) *International Journal of Nanomedicine* **7** 5725

[10] Gawande M B, Goswami A, Felpin F o-X, Asefa T, Huang X, Silva R, Zou X, Zboril R and Varma R S 2016 Cu and Cu-Based Nanoparticles: Synthesis and Applications in Catalysis *Chem. Rev* **116** 3722-811

[11] Son H Y, Ryu J H, Lee H and Nam Y S 2013 Bioinspired Templating Synthesis of Metal–Polymer Hybrid Nanostructures within 3D Electrospun Nanofibers *ACS applied materials & interfaces.* **5** 6381-90

[12] Dong H, Wang D, Sun G and Hinestroza J P 2008 Assembly of Metal Nanoparticles on Electrospun Nylon 6 Nanofibers by Control of Interfacial Hydrogen-Bonding Interactions *Chemistry of materials* **20** 6627-32
[13] He J, Zhao R, Zhang N, Lu X and Wang C 2018 Lightweight and flexible electrospun polymer nanofiber/metal nanoparticle hybrid membrane for high-performance electromagnetic interference shielding *NPG Asia Materials* **10** 749-60
[14] Mushibe E K, Andala D, Murphy S C, Raiti-Palazzolo K, Duffy-Matzner J L and Jones W E 2012 Electrically Conducting Polymers As Templating Interfaces for Fabrication of Copper Nanotubes *Langmuir* **28** 6684-90
[15] Barker B D 1981 Electroless deposition of metals *Surface Technology* **12** 77-88
[16] Testa A, Bernasconi R, Yoshikawa R, Takenaka I, Magagnin L and Shiratori S 2017 Transparent flexible electrodes based on junctionless copper nanowire network via selective electroless metallization of electrospun nanofibers *Journal of the Electrochemical Society* **164** D764-D70
[17] Hsu P-C, Kong D, Wang S, Wang H, Welch A J, Wu H and Cui Y 2014 Electrolessly deposited electrospun metal nanowire transparent electrodes *Journal of the American Chemical Society* **136** 10593
[18] Ji H, Zhao R, Li Y, Sun B, Li Y, Zhang N, Qiu J, Li X and Wang C 2018 Robust and durable superhydrophobic electrospun nanofibrous mats via a simple Cu nanocluster immobilization for oil-water contamination *Colloids and Surfaces A: Physicochemical and Engineering Aspects* **538** 173-83
[19] Yang X, Hu X, Wang Q, Xiong J, Yang H, Meng X, Tan L, Chen L and Chen Y 2017 Large-Scale Stretchable Semiembedded Copper Nanowire Transparent Conductive Films by an Electrospinning Template *ACS Appl. Mater. Interfaces* **9** 26468-75
[20] Paunovic M 2006 *Fundamentals of electrochemical deposition* (Hoboken, N.J.: Wiley-Interscience)
[21] Krulik G A 1982 TIN-PALLADIUM CATALYSTS FOR ELECTROLESS PLATING *Platinum Metals Review* **26** 58-64
[22] Lindsay J 2016 The characterization of the stannous chloride/ palladium chloride catalysts for electroless plating.(NASF TECHNICAL PAPERS) *Products Finishing* **80** 12
[23] Aminu T Q and Bahr D F 2018 Probing Adhesion of Metallic Nanoparticles on Polymeric Fibrous and Flat Architectures *MRS Advances* **3** 2749-56
[24] Kim G H, Woo H, Kim S, An T and Lim G 2020 Highly-robust, solution-processed flexible transparent electrodes with a junction-free electrospun nanofiber network *RSC Advances* **10** 9940-8
[25] Bakar S S S, Fong K C, Eleyas A and Nazeri M F M 2018 IOP conference series. Materials Science and Engineering. p 12076
[26] Godjevargova T, Simeonova A and Dimov A 2002 Adsorption of heavy metal ions from aqueous solutions by porous polyacrylonitrile beads *Journal of Applied Polymer Science* **83** 3036-44
[27] Zhou Z, Lai C, Zhang L, Qian Y, Hou H, Reneker D H and Fong H 2009 Development of carbon nanofibers from aligned electrospun polyacrylonitrile nanofiber bundles and characterization of their microstructural, electrical, and mechanical properties *Polymer* **50** 2999-3006
[28] Durmazel S, Üzer A e, Erbil B, Sayın B and Apak R a 2019 Silver Nanoparticle Formation-Based Colorimetric Determination of Reducing Sugars in Food Extracts via Tollens' Reagent *ACS Omega* **4** 7596-604
[29] Paglieri S N, Foo K Y, Way J D, Collins J P and Harper-Nixon D L 1999 A New Preparation Technique for Pd/Alumina Membranes with Enhanced High-Temperature Stability *Ind. Eng. Chem. Res* **38** 1925-36
[30] Schlesinger M and Paunovic M 2000 *Modern electroplating* (New York: Wiley)
[31] Reneker D H and Yarin A L 2008 Electrospinning jets and polymer nanofibers *Polymer* **49** 2387-425
[32] Reneker D H 2000 Bending instability of electrically charged liquid jets of polymer solutions in electrospinning *Journal of Applied Physics* **87** 4531-48

[33] Wei X and Roper D K 2014 Tin sensitization for electroless plating review *Journal of the Electrochemical Society* **161** D235-D42
[34] Krulik G A 1980 Hydrous melt catalyst synthesis *Journal of Catalysis* **65** 95-104
[35] Koo H C, Kim S Y, Cho S K and Kim J J 2008 Ag seed-layer formation by electroless plating for ultra-large-scale integration interconnection *Journal of the Electrochemical Society* **155** D558-D62
[36] Zhao M, Yu L, Akolkar R and Anderson A B 2016 Mechanism of electroless copper deposition from [Cu II EDTA] 2- complexes using aldehyde-based reductants *Journal of Physical Chemistry C* **120** 24789-93
[37] Baetzold R C 1983 Interaction of saturated hydrocarbons with transition-metal films: molecular orbital calculations *Journal of the American Chemical Society* **105** 4271-6
[38] Sung Y-C, Lai C-H, Lin S-J and Chang S-Y 2006 Early-Stage Nucleation Crystallography of Sensitization-Activated Palladium Catalysts and Electrolessly Deposited Copper Films *Electrochemical and Solid-State Letters* **9** C85-C7
[39] Chang S-Y, Hsu C-J, Fang R-H and Lin S-J 2003 Electrochemical deposition of nanoscaled palladium catalysts for 65 nm copper metallization *Journal of The Electrochemical Society* **150** C603
[40] Nørskov J K, Bligaard T, Logadottir A, Kitchin J R, Chen J G, Pandelov S and Stimming U 2005 Trends in the Exchange Current for Hydrogen Evolution *Journal of The Electrochemical Society* **152** J23
[41] Grouchko M, Kamyshny A, Ben-Ami K and Magdassi S 2009 Synthesis of copper nanoparticles catalyzed by pre-formed silver nanoparticles *An Interdisciplinary Forum for Nanoscale Science and Technology* **11** 713-6
[42] Li J, Su S, Zhou L, Kundrát V, Abbot A M, Mushtaq F, Ouyang D, James D, Roberts D and Ye H 2013 Carbon nanowalls grown by microwave plasma enhanced chemical vapor deposition during the carbonization of polyacrylonitrile fibers *Journal of Applied Physics* **113**
[43] Beyssac O, Goffé B, Petitet J-P, Froigneux E, Moreau M and Rouzaud J-N 2003 On the characterization of disordered and heterogeneous carbonaceous materials by Raman spectroscopy *Spectrochimica Acta Part A: Molecular and Biomolecular Spectroscopy* **59** 2267-76
[44] Muniz-Miranda M, Gellini C and Giorgetti E 2011 Surface-Enhanced Raman Scattering from Copper Nanoparticles Obtained by Laser Ablation *J. Phys. Chem. C* **115** 5021-7
[45] Lu Y, Liu G L and Lee L P 2005 High-Density Silver Nanoparticle Film with Temperature-Controllable Interparticle Spacing for a Tunable Surface Enhanced Raman Scattering Substrate *Nano Lett* **5** 5-9
[46] do Amaral Junior M A, Matsushima J T, Rezende M C, Gonçalves E S, Marcuzzo J S and Baldan M R 2017 Production and characterization of activated carbon fiber from textile PAN Fiber *Journal of Aerospace Technology and Management* **9** 423-30
[47] Ferrari A C and Robertson J 2001 Resonant Raman spectroscopy of disordered, amorphous, and diamondlike carbon *Physical review. B: Condensed matter.* **64** 075414
[48] Litmanovich A D and Platé N A 2000 Alkaline hydrolysis of polyacrylonitrile. On the reaction mechanism *Macromolecular Chemistry and Physics* **201** 2176-80
[49] Wang D, Yue Y, Wang Q, Cheng W and Han G 2020 Preparation of cellulose acetate-polyacrylonitrile composite nanofibers by multi-fluid mixing electrospinning method: Morphology, wettability, and mechanical properties *Applied surface science* **510** 145462
[50] Grassie N and McGuchan R 1970 Pyrolysis of polyacrylonitrile and related polymers—I. Thermal analysis of polyacrylonitrile *European Polymer Journal* **6** 1277-91
[51] Şahiner N, Pekel N and Güven O 1999 Radiation synthesis, characterization and amidoximation of N-vinyl-2-pyrrolidone/acrylonitrile interpenetrating polymer networks *Reactive and Functional Polymers* **39** 139-46
[52] Ren S, Dong L, Zhang X, Lei T, Ehrenhauser F, Song K, Li M, Sun X and Wu Q 2017 Electrospun Nanofibers Made of Silver Nanoparticles, Cellulose Nanocrystals, and Polyacrylonitrile as Substrates for Surface-Enhanced Raman Scattering *Materials (Basel)* **10** 68

[53] Onwudiwe D C, Strydom C A, Vala R M K and Tichagwa L 2015 Preparation and Structural Properties of Electrospun PAN Nanofibers Reinforced With ZnS Nanoparticles *Synthesis and reactivity in inorganic, metal-organic, and nano-metal chemistry* **45** 1251-9
[54] Warrier P and Teja A 2011 Effect of particle size on the thermal conductivity of nanofluids containing metallic nanoparticles *Nanoscale Res Lett* **6** 1-6

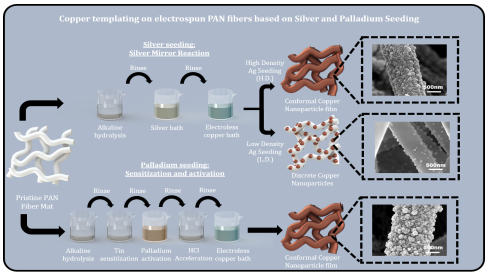

GRAPHICAL ABSTRACT

CONTROL OF COPPER NANOPARTICLE METALLIZATION ON ELECTROSPUN FIBERS VIA PD AND AG SEED-ASSISTED TEMPLATING

SUPPLEMENTARY INFORMATION

Temitope Q. Aminu (taminu@purdue.edu), David F. Bahr (dfbahr@purdue.edu)

School of Materials Engineering, Purdue University, West Lafayette, IN 47907, U.S.A.

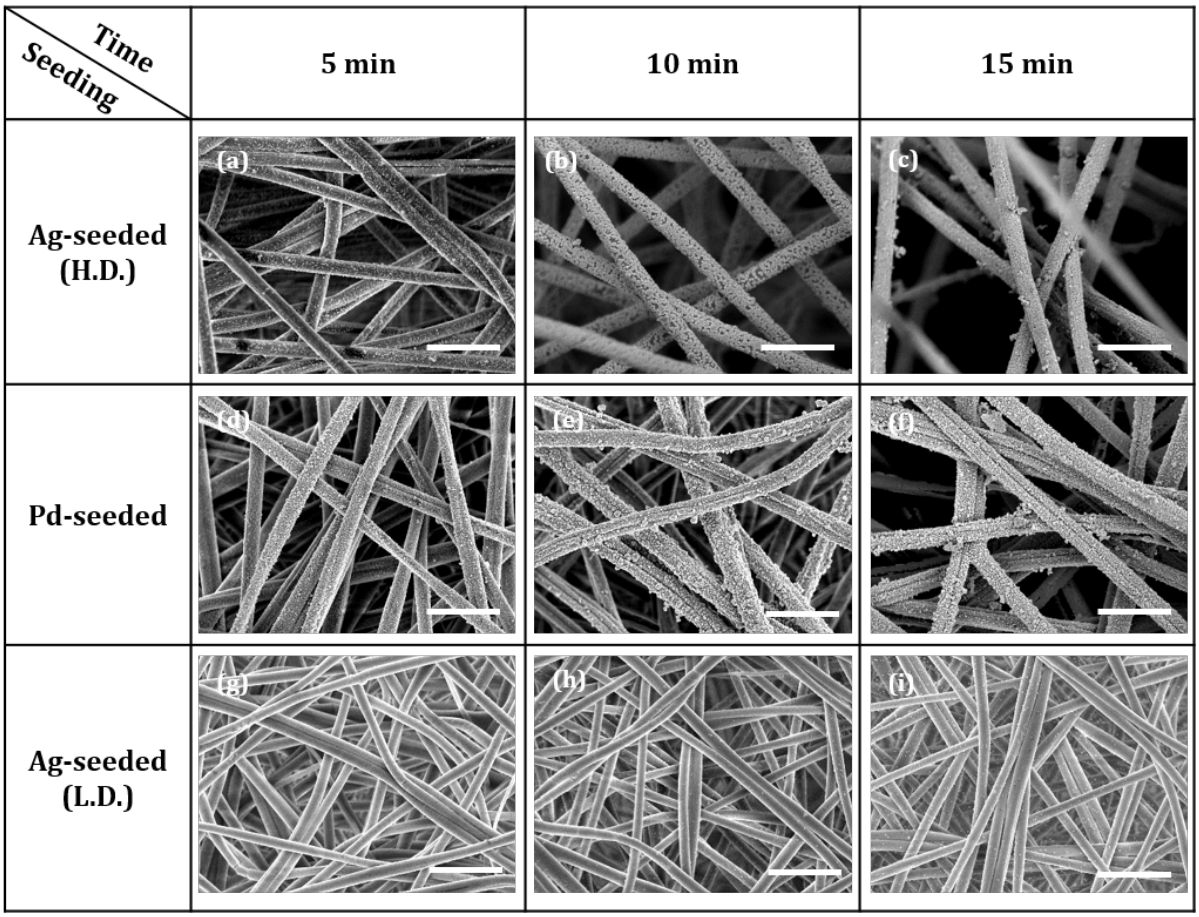

Figure S1: Global SEM view of copper nanoparticle evolution on the seeded fibers (a) PAN-Ag-Cu-5 (b) PAN-Ag-Cu-10 (c) PAN-Ag-Cu-15 for High density seeding; (d) PAN-Pd-Cu-5 (e) PAN-Pd-Cu-10 (f) PAN-Pd-Cu-15 for Pd seeding. (g) PAN-Ag-Cu-5 (h) PAN-Ag-Cu-10 (i) PAN-Ag-Cu-15 for low density seeding. Scale bar is 5 µm

Author accepted version, Journal of Materials Science, vol. 56, pp 16307-16323(2021)
DOI: 10.1007/s10853-021-06326-x

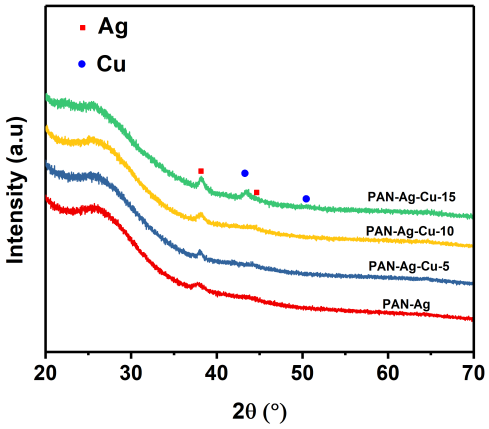

Figure S2: X-ray diffraction pattern for copper evolution on low-density silver seeded PAN fibers

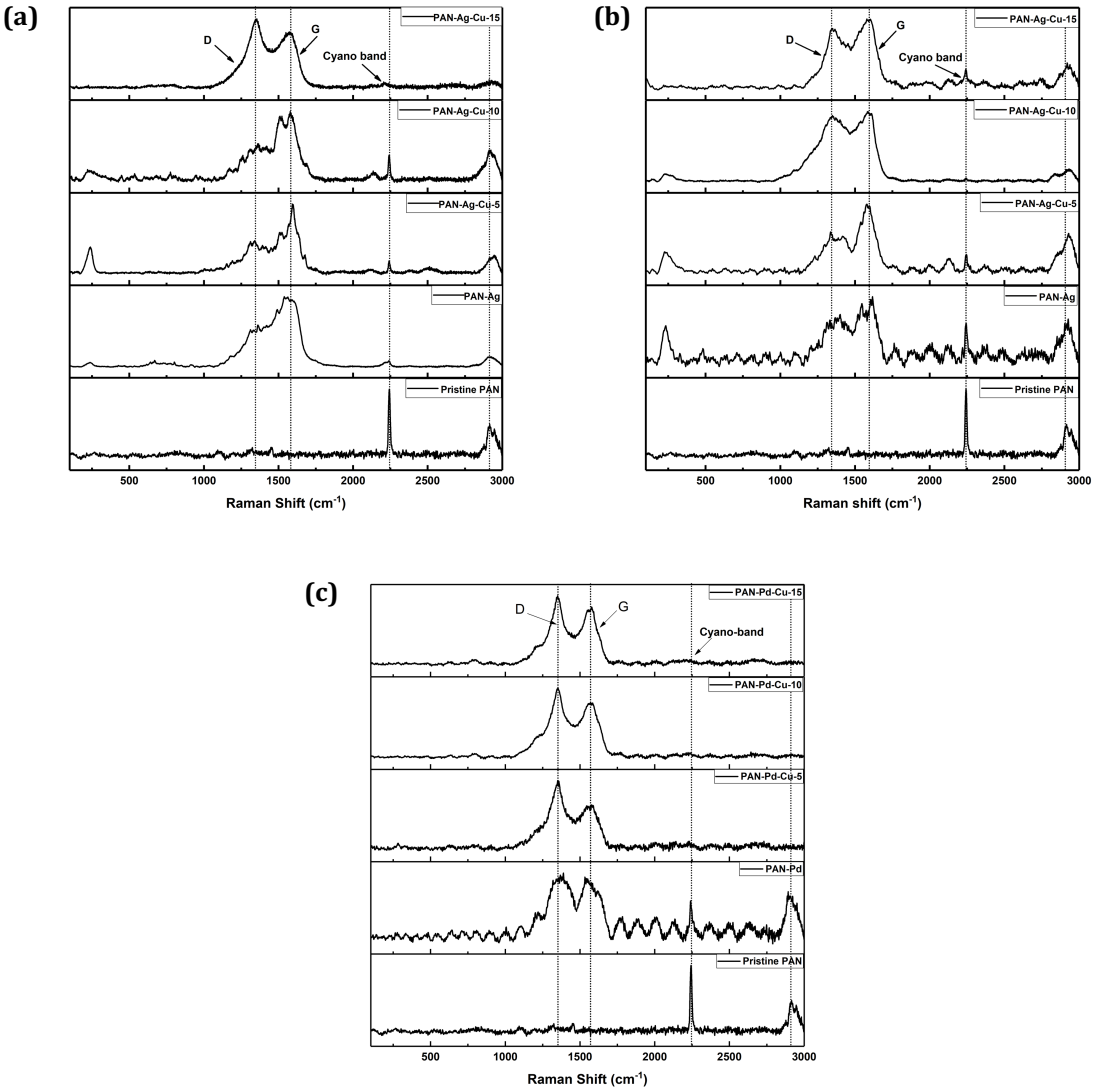

Figure S3: Complete Raman shifts for time-resolved copper NP evolution on PAN fibers with (a) Ag-seeding (H.D.) (b) Ag-seeding (L.D.) (c) Pd seeding

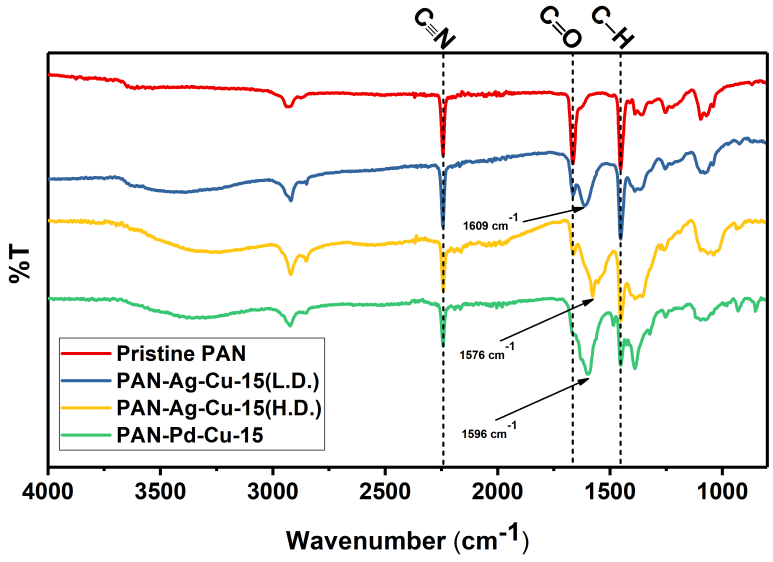

Figure S4: FTIR spectra of PAN, PAN-Ag-Cu-15 (L.D.), PAN-Ag-Cu-15 (H.D.), and PAN-Pd-Cu-15

In general, the pure PAN, PAN-Ag-Cu-15 (L.D.), PAN-Ag-Cu-15 (H.D.), PAN-Pd-Cu-15 show characteristic bands at 2930 cm^{-1} attributed to stretching of the ν(C – H) in (–CH_2 –); at 2240 cm^{-1} from stretching of the cyano functional group, υ(C≡N); and at 1451 cm^{-1} due to δ(C–H) bending. The band corresponding to υ(C=O) at 1665 cm^{-1} is possibly from the carbonyl groups in dimethylformamide and acetone used as solvents for the electrospinning solution. Specifically, the Cu metallized samples exhibited distinct peaks from 1615 – 1565 cm^{-1}, attributable to υ(C=C) stretching, and υ(C=N) stretching in pyridine structures [1]. This suggests a cyclization of the nitrile groups in polyacrylonitrile, creating pyridine-like repeat molecular structures.

Reference

[1] Stuart B H 2004 *Infrared Spectroscopy Fundamentals and Applications* (Chichester: Wiley)